WAVELETS, A NUMERICAL TOOL FOR MULTISCALE PHENOMENA: FROM TWO DIMENSIONAL TURBULENCE TO ATMOSPHERIC DATA ANALYSIS.

PATRICK FISCHER AND KA-KIT TUNG

Abstract. Multiresolution methods, such as the wavelet decompositions, are increasingly used in physical applications where multiscale phenomena occur. We present in this paper two applications illustrating two different aspects of the wavelet theory.

In the first part of this paper, we recall the bases of the wavelets theory. We describe how to use the continuous wavelet decomposition for analyzing multifractal patterns. We also summarize some results about orthogonal wavelets and wavelet packets decompositions.

In the second part, we show that the wavelet packet filtering can be successfully used for analyzing two-dimensional turbulent flows. This technique allows the separation of two structures: the solid rotation part of the vortices and the remaining mainly composed of vorticity filaments. These two structures are multiscale and cannot be obtained through usual filtering methods like Fourier decompositions. The first structures are responsible for the inverse transfer of energy while the second ones are responsible for the forward transfer of enstrophy. This decomposition is performed on numerical simulations of a two dimensional channel in which an array of cylinders perturb the flow.

In the third part, we use a wavelet-based multifractal approach to describe qualitatively and quantitatively the complex temporal patterns of atmospheric data. Time series of geopotential height are used in this study. The results obtained for the stratosphere and the troposphere show that the series display two different multifractal behaviors. For large time scales (several years), the main Hölder exponent for the stratosphere and the troposphere data are negative indicating the absence of correlation. For short time scales (from few days to one year), the stratopshere series present some correlations with Hölder exponents larger than 0.5, whereas the troposhere data are much less correlated.

Key Words. Wavelets, two dimensional turbulence, multifractal analysis, atmospheric data

1. Review on wavelets

The one dimensional wavelet theory is reviewed in this part. The generalization to higher dimension is relatively easy and is based on tensor products of one dimensional basis functions. The two dimensional wavelet theory is recalled here in the wavelet packets framework only. We present here a summary of the theory, and a more complete description can be found in [12, 26].

Any time series, which can be seen as a one dimensional mathematical function, can

be represented by a sum of fundamental or simple functions called basis functions. The most famous example, the Fourier series,

$$s(t) = \sum_{k=-\infty}^{+\infty} c_k e^{ikt}$$

is valid for any 2π -periodic function sufficiently smooth. Each basis function, e^{ikt} is indexed by a parameter k which is related to a frequency. In (1), s(t) is written as a superposition of harmonic modes with frequencies k. The coefficients c_n are given by the integral

$$(2) c_k = \frac{1}{2\pi} \int_0^{2\pi} s(t)e^{-ikt}dt$$

Each coefficient c_k can be viewed as the average harmonic content of s(t) at frequency k. Thus the Fourier decomposition gives a frequency representation of any signal. The computation of c_k is called the decomposition of s and the series on the right hand side of (1) is called the reconstruction of s.

Although this decomposition leads to good results in many cases, some disadvantages are inherent to the method. One of them is the fact that all the information concerning the space behaviour of the signal is completely lost in the Fourier description. For instance, a discontinuity or a localised high variation of the frequency will not be well described by the Fourier representation. The underlying reason lies in the nature of complex exponential functions used as basis functions. They all cover the entire real line, and differ only with respect to frequency. They are not suitable for representing the behaviour of a discontinuous function or a signal with high localised oscillations.

Like the complex exponential functions of the Fourier decomposition, wavelets can be used as basis functions for the representation of a signal. But, unlike the complex exponential functions, they are able to restore the positional information as well as the frequency information.

1.1. Continuous wavelets and the multifractal formalism. The wavelet-based multifractal formalism has been introduced in the nineties by Mallat [25, 26], Arneodo [2, 3, 4], Bacry [5] and Muzy [28]. A wavelet transform can focus on localized signal structures with a zooming procedure that progressively reduces the scale parameter. Singularities and irregular structures often correspond to essential information in a signal. The local signal regularity can be described by the decay of the wavelet transform amplitude across scales. Singularities can be detected by following the wavelet transform local maxima at fine scales.

The wavelet transform is a convolution product of a data sequence with the compressed (or dilated) and translated version of a basis function ψ called the wavelet mother. The scaling and translation are performed by two parameters: the scale parameter a dilates or compresses the mother wavelet to various resolutions and the translation parameter b moves the wavelet all along the sequence:

(3)
$$WT_s(b,a) = \frac{1}{\sqrt{a}} \int_{-\infty}^{+\infty} s(t)\psi^*\left(\frac{t-b}{a}\right) dt, \ a \in \mathbb{R}^{+*}, b \in \mathbb{R}.$$

This definition of the wavelet transform leads to an invariant L^2 measure, and thus conserves the energy ($||s||_2 = ||WT_s||_2$). A different normalization could be used leading to a different invariant.

The strength of a singularity of a function is usually defined by an exponent called Hölder exponent. The Hölder exponent $h(t_0)$ of a function s at the point t_0 is defined as the largest exponent such that there exists a polynomial $P_n(t)$ of order n satisfying:

$$(4) |s(t) - P_n(t - t_0)| \le C|t - t_0|^{h(t_0)},$$

for t in a neighborhood of t_0 . The order n of the polynomial P_n has to be as large as possible in (4). The polynomial P_n can be the Taylor expansion of s around t_0 . If $n < h(t_0) < n+1$ then s is C^n but not C^{n+1} . The exponent h evaluates the regularity of s at the point t_0 . The higher the exponent h, the more regular the function s. It can be interpreted as a local measure of 'burstiness' in the timeseries at time t_0 . A wavelet transform can estimate this exponent by ignoring the polynomial P_n . A transcient structure or 'burst' is generally wavelet-transformed to a superposition of wavelets with the same centre of mass and wide range of frequencies.

In order to evaluate the Hölder exponent, we have to choose a wavelet mother with m > h vanishing moments:

(5)
$$\int_{-\infty}^{\infty} t^k \psi(t) dt,$$

for $0 \le k < m$. A wavelet with m vanishing moments is orthogonal to polynomials of degree m-1. Since h < m, the polynomial P_n has a degree n at most equal to m-1 and we can then show that:

(6)
$$\int_{-\infty}^{+\infty} P_n(t - t_0) \psi^* \left(\frac{t - b}{a}\right) dt = 0.$$

Let us assume that the function s can be written as a Taylor expansion around t_0 :

(7)
$$s(t) = P_n(t - t_0) + C|t - t_0|^{h(t_0)}$$

We then obtain for its wavelet transform at t_0 :

(8)
$$WT_s(t_0, a) = \frac{1}{\sqrt{a}} \int_{-\infty}^{+\infty} C|t - t_0|^{h(t_0)} \psi^* \left(\frac{t - t_0}{a}\right) dt$$

(9)
$$= C|a|^{h(t_0)+\frac{1}{2}} \int_{-\infty}^{+\infty} |t'|^{h(t_0)} \psi(t') dt'.$$

We have the following power law proportionality for the wavelet transform of the singularity of $s(t_0)$:

(10)
$$|WT_s(t_0, a)| \sim a^{h(t_0) + \frac{1}{2}}$$

Then, we can evaluate the exponent $h(t_0)$ from a log-log plot of the wavelet transform amplitude versus the scale a.

However, we cannot compute the regularity of a multifractal signal because its singularities are not isolated. But we can still obtain the singularity spectrum of multifractals from the wavelet transform local maxima.

These maxima are located along curves in the plane (b, a). This method, introduced by Arneodo et al. [3], requires the computation of a global partition function Z(q, a). Let $\{b_i(a)\}_{i\in\mathbb{Z}}$ be the position of all maxima of $|WT_s(b, a)|$ at a fixed scale a. The partition function Z(q, a) is then defined by:

(11)
$$Z(q, a) = \sum_{i} |WT_{s}(b_{i}, a)|^{q}.$$

We can then assess the asymptotic decay $\tau(q)$ of Z(q, a) at fine scales a for each $q \in \mathbb{R}$:

(12)
$$\tau(q) = \lim_{a \to 0} \inf \frac{\log Z(q, a)}{\log a}.$$

This last expression can be rewritten as a power law for the partition function Z(q, a):

(13)
$$Z(q,a) \sim a^{\tau(q)}.$$

If the exponents $\tau(q)$ define a straight line than the signal is a monofractal, otherwise the signal is called multifractal: the regularity properties of the signal are inhomogeneous, and change with location.

Finding the distribution of singularities in a multifractal signal is necessary for analyzing its properties. The so-called spectrum of singularity D(h) measures the repartition of singularities having different Hölder regularity. The singularity spectrum D(h) gives the proportion of Hölder h type singularities that appear in the signal. A fractal signal has only one type of singularity, and its singularity spectrum is reduced to one point. The singularity spectrum D(h) for any multifractal signal can be obtained from the Legendre transform of the scaling exponent $\tau(q)$ previously defined:

(14)
$$D(h) = \min_{q \in \mathbb{R}} \left(q(h + \frac{1}{2}) - \tau(q) \right).$$

Let us notice that this formula is only valid for functions with a convex singularity spectrum [26]. In general, the Legendre transform gives only an upper bound of D(h) [18, 19]. For a convex singularity spectrum D(h), its maximum

(15)
$$D(h_0) = \max_h D(h) = -\tau(0)$$

is the fractal dimension of the Hölder exponent h_0 .

Remark: When the maximum value of the wavelet transform modulus is very small, the formulation of the partition function given in (11) can diverge for q < 0. A way to avoid this problem consists in replacing the value of the wavelet transform modulus at each maximum by the supremum value along the corresponding maxima line at scales smaller than a:

(16)
$$Z(q,a) = \sum_{l \in \mathcal{L}(a)} \left(\sup_{(t,a') \in l, a' < a} |WT_s(t,a)| \right)^q,$$

where $\mathcal{L}(a)$ is the set of all maxima lines l satisfying: $l \in \mathcal{L}(a)$, if $\forall a' \leq a, \exists (x, a') \in l$. The properties of this modified partition function are well described in [3].

1.2. One-dimensional orthogonal wavelet bases. The theoretical construction of orthogonal wavelet families is intimately related to the notion of Multiresolution Analysis [25]. A Multiresolution Analysis is a decomposition of the Hilbert space $L^2(\mathbb{R})$ of physically admissible functions (i.e square integrable functions) into a chain of closed subspaces,

$$\ldots \subset V_2 \subset V_1 \subset V_0 \subset V_{-1} \subset V_{-2} \ldots$$

such that

•
$$\bigcap_{j\in\mathbb{Z}}V_j=\{0\}$$
 and $\bigcup_{j\in\mathbb{Z}}V_j$ is dense in $L^2(\mathbb{R})$

- $f(x) \in V_j \Leftrightarrow f(2x) \in V_{j-1}$
- $f(x) \in V_0 \Leftrightarrow f(x-k) \in V_0$
- There is a function $\varphi \in V_0$, called the father wavelet, such that $\{\varphi(x-k)\}_{k\in\mathbb{Z}}$ is an orthonormal basis of V_0

Let W_j be the orthogonal complementary subspace of V_j in V_{j-1} :

$$(17) V_i \oplus W_i = V_{i-1}$$

This space contains the difference in information between V_j and V_{j-1} , and allows the decomposition of $L^2(\mathbb{R})$ as a direct form:

$$(18) L^2(\mathbb{R}) = \bigoplus_{j \in \mathbb{Z}} W_j$$

Then, there exists a function $\psi \in W_0$, called the mother wavelet, such that $\{\psi(x-k)\}_{k\in\mathbb{Z}}$ is an orthonormal basis of W_0 . The corresponding wavelet bases are then characterized by:

(19)
$$\varphi_{i,k}(x) = 2^{-j/2} \varphi(2^{-j}x - k), \quad k, j \in \mathbb{Z},$$

(20)
$$\psi_{j,k}(x) = 2^{-j/2}\psi(2^{-j}x - k), \quad k, j \in \mathbb{Z}.$$

Given an integer M, it is possible to select a mother wavelet such that:

(21)
$$\int_{\mathbb{R}} dx \, \psi(x) \, x^m = 0, \quad m = 0, \dots, M - 1 \,,$$

which means that it has M vanishing moments and the approximation order of the wavelet transform is then also M.

Since the scaling function $\varphi(x)$, and the mother wavelet $\psi(x)$ belong to V_{-1} , they admit the following expansions:

(22)
$$\varphi(x) = \sqrt{2} \sum_{k=0}^{L-1} h_k \, \varphi(2x - k), \quad h_k = \langle \varphi, \varphi_{-1,k} \rangle ,$$

(23)
$$\psi(x) = \sqrt{2} \sum_{k=0}^{L-1} g_k \varphi(2x - k), \quad g_k = (-1)^k h_{L-k-1} ,$$

where the number L of coefficients is connected to the number M of vanishing moments and is also connected to other properties that can be imposed to $\varphi(x)$. The families $\{h_k\}$ and $\{g_k\}$ form in fact a conjugate pair of quadrature filters H and G. Functions verifying (22) or (23) have their support included in $[0, \ldots, L-1]$. Furthermore, if there exists a coarsest scale, j=n, and a finest one, j=0, the bases can be rewritten as:

(24)
$$\varphi_{j,k}(x) = \sum_{l=0}^{L-1} h_l \, \varphi_{j-1,2k+l}(x), \quad j = 1, \dots, n ,$$

and

(25)
$$\psi_{j,k}(x) = \sum_{l=0}^{L-1} g_l \, \varphi_{j-1,2k+l}(x), \quad j = 1, \dots, n.$$

The wavelet transform of a function f(x) is then given by two sets of coefficients defined as

(26)
$$d_k^j = \int_{\mathbb{R}} dx f(x) \psi_{j,k}(x) ,$$

and

(27)
$$r_k^j = \int_{\mathbb{R}} dx \, f(x) \, \varphi_{j,k}(x) .$$

Starting with an initial set of coefficients r_k^0 , and using (24) and (25), coefficients d_k^j and r_k^j can be computed by means of the following recursive relations:

(28)
$$d_k^j = \sum_{l=0}^{L-1} g_l \, r_{2k+l}^{j-1} \;,$$

and

(29)
$$r_k^j = \sum_{l=0}^{L-1} h_l \, r_{2k+l}^{j-1} .$$

Coefficients d_k^j , and r_k^j are considered in (28) and (29) as periodic sequences with the period 2^{n-j} . The set d_k^j , is composed by coefficients corresponding to the decomposition of f(x) on the basis $\psi_{j,k}$ and r_k^j may be interpreted as the set of averages at various scales.

1.3. One-dimensional wavelet packets. Let H and G be a conjugate pair of quadrature filters whose the coefficients are respectively denoted by h_j and g_j . One denotes by ψ_0 and ψ_1 the corresponding father and mother wavelets. The following sequence of functions can be defined using the filters H and G:

(30)
$$\psi_{2n}(x) = \sqrt{2} \sum_{j \in \mathbb{Z}} h_j \psi_n(2x - j),$$
$$\psi_{2n+1}(x) = \sqrt{2} \sum_{j \in \mathbb{Z}} g_j \psi_n(2x - j).$$

The set of these functions $\{\psi_n\}_n$ defines the wavelet packets associated to H and G. An orthonormal wavelet packet basis of $L^2(\mathbb{R})$ is any orthonormal basis selected from among the functions $2^{s/2}\psi_n(2^sx-j)$. The selection process, the so-called Best Basis algorithm, will be described in the sequel. Each basis element is characterized by three parameters: scale s, wavenumber n and position j. A useful representation of the set of wavelet packet coefficients is that of a rectangle of dyadic blocks. For instance, if one considers a signal defined at 8 points $\{x_1, ..., x_8\}$, then the wavelet packet coefficients of this function can be summarized by Table 1.

x_1	x_2	x_3	x_4	x_5	x_6	x_7	x_8
r_1	r_2	r_3	r_4	d_1	d_2	d_3	d_4
rr_1	rr_2	dr_1	dr_2	rd_1	rd_2	dd_1	dd_2
rrr_1	drr_1	rdr_1	ddr_1	rrd_1	drd_1	rdd_1	ddd_1

Table 1. Dyadic blocks of wavelet packet coefficients

Each row is obtained by the application of either filter H or G to the previous row. The application of H is denoted by r as "resuming" and the application of G by d as "differencing". For instance, the set $\{rd_1 \quad rd_2\}$ is obtained by the application of the filter H to $\{d_1 \quad d_2 \quad d_3 \quad d_4\}$, and $\{dd_1 \quad dd_2\}$ by the application of the filter G. The so called Daubechies wavelets defined in [12] with several numbers of vanishing moments have been used in the sequel.

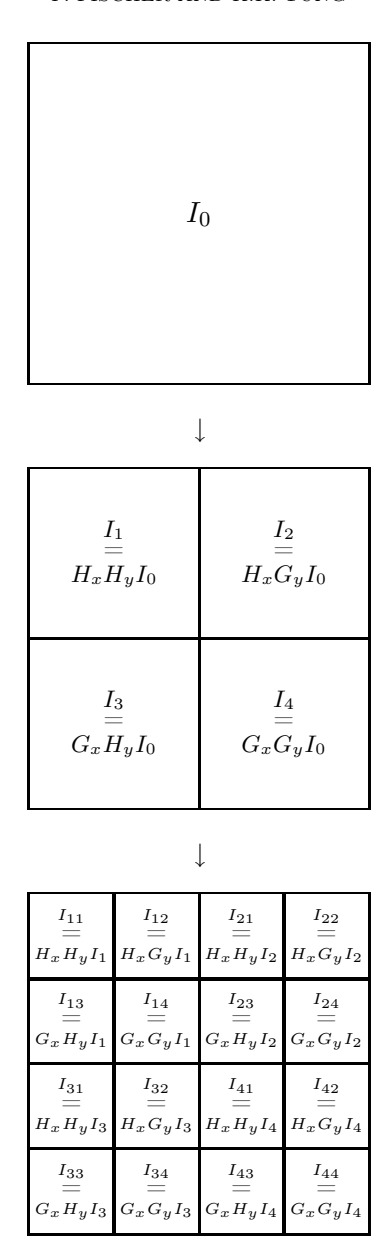


FIGURE 1. Two levels of two dimensional wavelet packets decomposition

1.4. Two-dimensional packets and the best basis algorithm. Two-dimensional wavelet packets can be obtained by tensor products $\psi_{snk}(x).\psi_{s'n'k'}(y)$ of one-dimensional basis elements. The support of these functions is exactly the cartesian product of the supports of $\psi_{snk}(x)$ and $\psi_{s'n'k'}(y)$. The same scale s=s' will be used in the sequel. Subsets of such functions can be indexed by dyadic squares, with the squares corresponding to the application of one of the following filters $H \otimes H = H_x H_y$, $H \otimes G = H_x G_y$, $G \otimes H = G_x H_y$, or $G \otimes G = G_x G_y$. A graphical representation of a two-dimensional wavelet packets decomposition is given in Figure 1.

Arrays of wavelet packets constitute huge collections of basis from which one has to choose and pick. The main criterion consists in seeking a basis in which the coefficients, when rearranged into decreasing order, decrease as fast as possible. Several numerical criteria do exist and one refers to [31] for more details. The *entropy* has been chosen since it is the more often used for this type of application. For a given one-dimensional vector $u = \{u_k\}$, it is defined as:

(31)
$$E(u) = \sum_{k} p(k) \log(\frac{1}{p(k)}),$$

where $p(k) = \frac{|u_k|^2}{\|u\|^2}$ is the normalized energy of the k^{th} element of the vector under study. If p(k) = 0 then we set $p(k) \log(\frac{1}{p(k)}) = 0$. All the terms in the sum are positive. In fact, the *entropy* measures the logarithm of the number of meaningful coefficients in the original signal. The vector $p = \{p(k)\}_k$ can be seen as a discrete probability distribution function since $0 \le p(k) \le 1$, $\forall k$ and $\sum_k p(k) = 1$. It can be easily shown that if only N of the values p(k) are nonzero, then $E(u) \leq \log N$. Such a probability distribution function is said to be concentrated into at most Nvalues. If E(u) is small then we may conclude that u is concentrated into a few values of p(k), with all other values being rare. The overabundant set of coefficients is naturally organized into a quadtree of subspaces by frequency. Every connected subtree containing the root corresponds to a different orthonormal basis. The most efficient of all the bases in the set may be found by recursive comparison: the choice algorithm will find the global minimum in O(N) operations, where N is the initial degree of freedom number. In fact, the basis is chosen automatically to best represent the original data. Hence the name best basis. Routines in Matlab written by D. Donoho [13] and based on the algorithms designed by M.V. Wickerhauser are used for performing the packets decompositions and for searching for the best bases.

2. Application to two dimensional turbulence

While three dimensional turbulence is governed by a direct cascade of energy from the scale of injection to the small scales where the energy is dissipated, two dimensional turbulence admits two different ranges [7, 22, 23]. The first one, at large scales, is governed by an inverse energy cascade from the scale of injection to the large scales. The second one, at small scales, is governed by a cascade of enstrophy from the scale of injection to the small scales. This scenario, proposed by Kraichnan and Batchelor over 40 years ago, finds confirmation in different numerical simulations and experimental realizations. However, if the scaling laws for the different ranges have found some confirmation, the structures responsible for such transfers have not been completely identified.

Two dimensional turbulence has interested and continues to interest different scientific communities. Its relevance to atmospheric and oceanic flows at large scales has largely motivated its detailed study [24, 27, 30]. Numerical simulations have, for much longer, identified several features of 2D turbulent flows. Now, it appears that two cascades exist in a two dimensional turbulent flow. An inverse energy cascade due to the merging of like sign vortices transfers energy from the injection scale to the large scales. At scales smaller than this injection scale, an enstrophy cascade, whose origin is apparently the straining of vorticity gradients, transfers enstrophy from the large to the small scales. While the role of vortices has been identified as crucial for the dynamics of 2D flows, there has been only few if any studies of

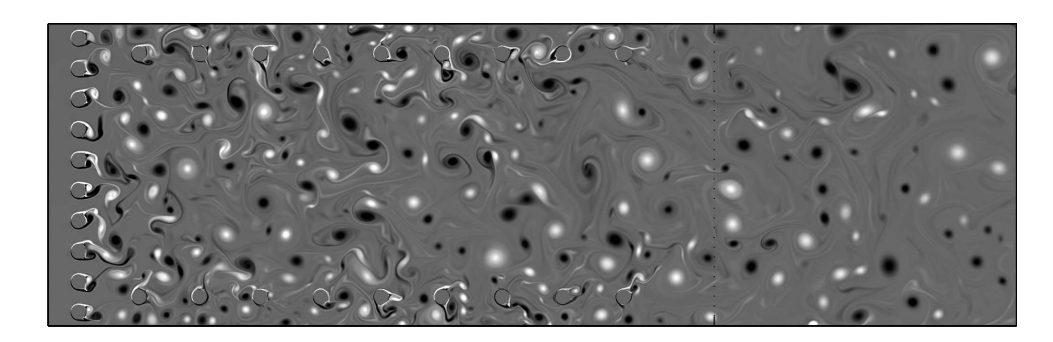


FIGURE 2. Snapshot of the vorticity field with the selected domain of analysis at the end of the channel delimited by a dotted line.

the role of flow structures on the transfers of either energy or enstrophy. This is precisely what we show here using two dimensional wavelet packets decompositions.

2.1. Numerical setup. Direct numerical simulations are used to obtain a two dimensional turbulent flow at relatively high Reynolds numbers. This flow is obtained in a channel with a length of either four or five times its width and where the turbulence is generated by arrays of cylinders. This configuration has been studied recently and the complete results have been reported in [9, 14, 15]. These simulatilons have been originally motivated by experiments carried out with soap films where grid turbulence was studied in detail [21, 20]. In order to keep a cartesian mesh, on which accurate finite differences schemes are written [11], the solid obstacles are considered as a porous medium of very weak permeability. So, instead of the classical Navier-Stokes equations, the following penalized Navier-Stokes equations [1, 10] are solved:

(32)
$$\partial_t U + (U \cdot \nabla) U - \frac{1}{Re} \Delta U + \frac{U}{K} + \nabla p = 0$$
(33)
$$div U = 0$$

where U = (u, v) is the velocity, p the pressure, Re the nondimensional Reynolds number based on the unit inlet flowrate and length and K the nondimensional coefficient of permeability of the medium. The fluid and the solid media correspond to an infinite and a zero permeability coefficient respectively, $K=10^{16}$ and K= 10^{-8} are the approximate values used in the numerical simulation. The above equations are associated to no-slip boundary conditions on the walls of the channel, Poiseuille flow on the entrance section and a non reflecting boundary condition on the exit section [8]. A typical snapshot of such a simulation is presented in Figure 2 where the cylinders are apparent both near the side walls and at one distance down from the entrance. This is the flow field we analyze here using using techniques based on wavelet analysis. Contrary to standard Fourier analysis, the wavelet decomposition we use here reveals the different structures of the flow at all spatial scales. This is also different from other filtering techniques where averaging over a certain range of scales is carried out. The overall filtering process can be summarized as follows:

(1) Computation of the wavelet packets decomposition of the two components of the velocity $U = (u_1, u_2)$.

- (2) Separation of the velocity fields into two subfields: the first subfield $U_s = (u_{1s}, u_{2s})$ corresponds to the wavelet packet coefficients with a modulus larger than a given threshold ϵ , and the second one $U_f = (u_{1f}, u_{2f})$ corresponds to the wavelet packet coefficients with a modulus smaller than ϵ .
- (3) Construction of the corresponding vorticity fields, ω_s and ω_f . The filtered field ω_s is then essentially composed by the solid rotation part of the vortices, and the filtered field ω_f by the vorticity filaments in between that roll up in spirals inside the vortices.
- (4) Computations of the physical data: energy and enstrophy spectra and fluxes.
- **2.2.** Computation of the energy and enstrophy spectra. In this section is presented the main result concerning the analysis of the role of each filtered subfield to the two-dimensional turbulence mechanism.

The velocity decomposition $U = U_s + U_f$ obtained with the wavelet packets based filtering is orthogonal and leads to the energy spectrum decomposition

(34)
$$E(k) = E_s(k) + E_f(k),$$

where E_s is the energy of the solid rotation vortices and E_f is the energy of the vorticity filaments, as can be verified on Figure 3. We observe that both subfields

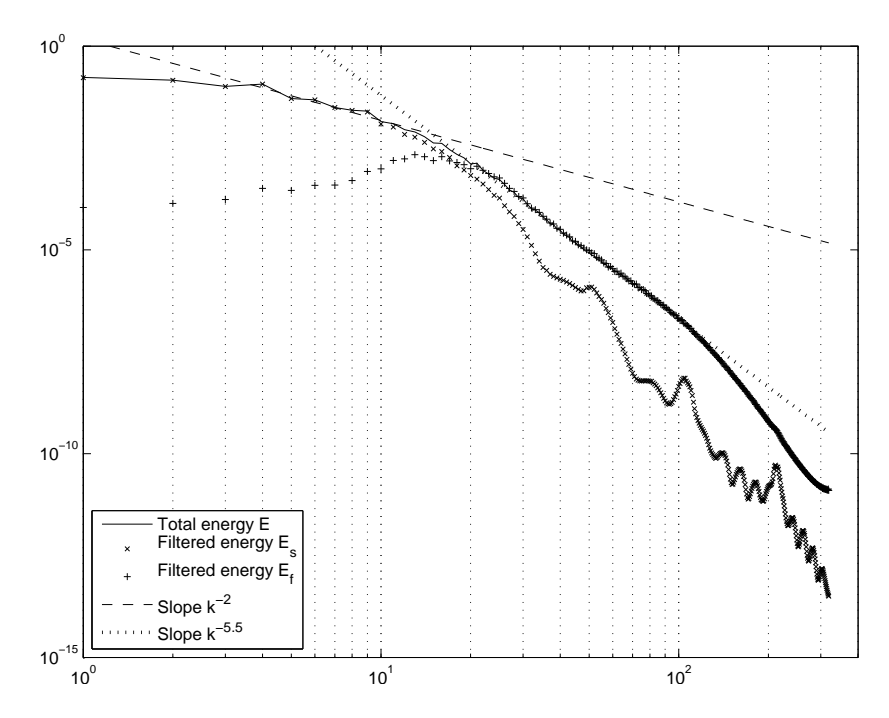


FIGURE 3. Energy spectra of the original and filtered fields obtained by a 5 scales wavelet packets decomposition $(k_{inj} \approx 20)$.

are multiscale even if the E_s spectrum dominates before the injection scale and the E_f spectrum dominates after the injection scale. And the filtered energy spectra are superimposed to the global energy spectrum when they dominate. A first slope in k^{-2} and a second one in $k^{-5.5}$ on both sides of the injection scale are obtained. The first slope is not really clear as it is short but the second one is obvious.

The same decomposition of the enstrophy spectrum yields a behavior in k^0 and $k^{-3.5}$ respectively as can be observed on Figure 4. The decomposition into the

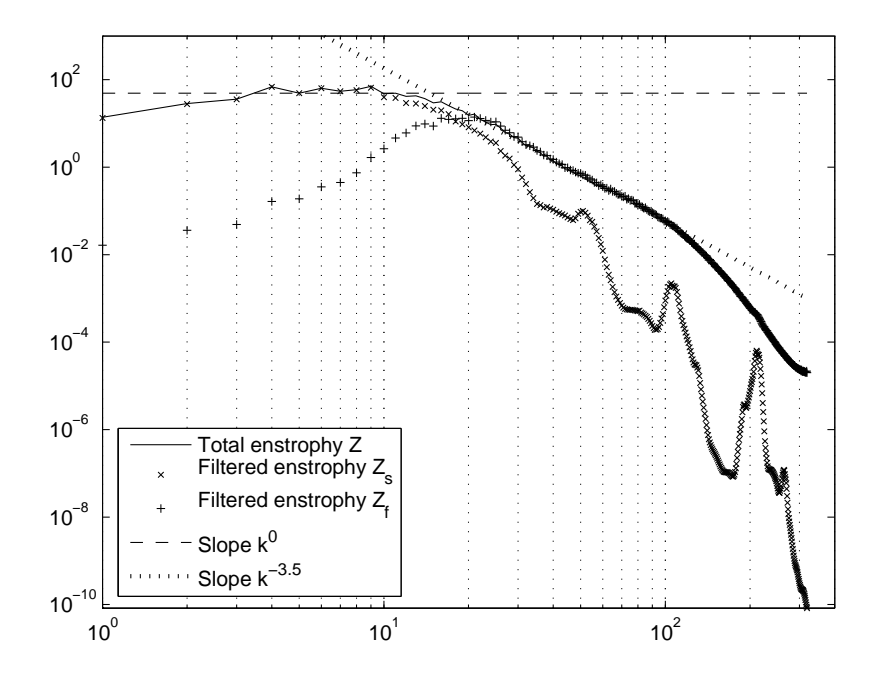


FIGURE 4. Original and filtered (WP 5 scales) enstrophy spectra $(k_{inj} \approx 20)$.

two subfields obtained by the wavelet packets filtering process is given in Figure 5. The solid rotation subfield ω_s reveals all the vortices with a smooth transition and the vorticity filaments subfield ω_f shows the vorticity filaments between the vortices that end up in spirals inside the vortices. Both subfields are continuous and multiscale. The first subfield is obtained with less than 1% of the coefficients of the decomposition. It contains more than 95% of the total energy and around 70% of the enstrophy while the second one contains less than 5% of the total energy but around 30% of the enstrophy. This distribution of the enstrophy shows that unfortunately the whole flow can not be represented properly only by the first subfield. Indeed, when the vorticity filaments subfield is neglected, the global motion cannot be correct. In contrast with a Fourier based filtering, the present orthogonal filtering does not separate the scales of the flow but the type of sctructures. Here the two subfields are not seen like vortical coherent structures and background as done in previous studies but like two coherent and multiscale subfields with their own dynamics. The purpose of this paper is not the detailed study of two dimensional turbulent flows, but to show two applications of wavelet based methods. The reader particularly interested in two dimensional turbulence will find more results in [14, 15, 16].

2.3. Discussion. A careful analysis of the flows using wavelet packets filtering on sufficient levels yields relevant results one can trust. Using an adapted threshold on the wavelet coefficients allows to separate the flow into two continuous and

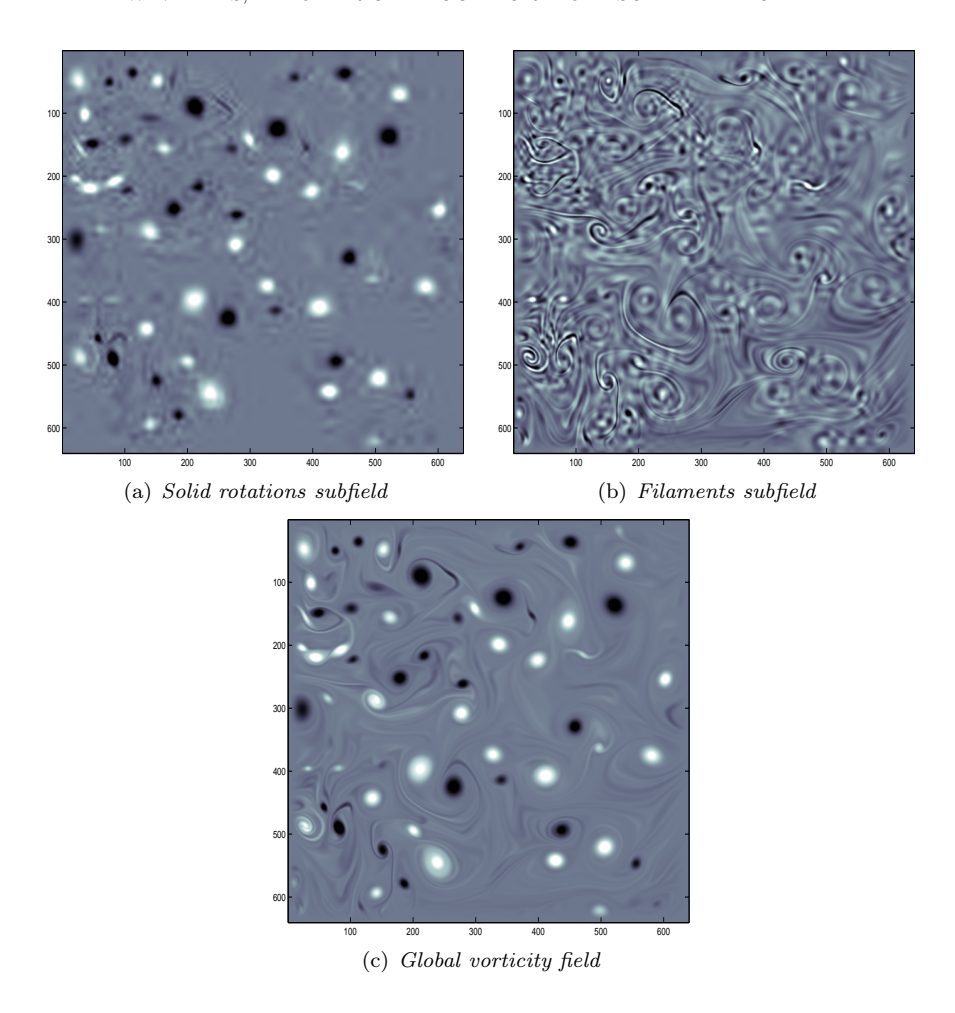


FIGURE 5. Wavelet packets filtering of a snapshot at the end of the channel $(k_{inj} \approx 20)$.

multiscale subfields, on one hand the solid rotation of the vortices and on the other hand the vorticity filaments that connect the vortices and roll up in spirals inside the vortices. The second subfield cannot be neglected as it contains around 30% of the enstrophy and contributes for a significant part of the motion of the whole flow.

3. Multifractal analysis of atmospheric time series

Depending on the application, there are various ways of computing the wavelet transform. For the purpose of compression for instance, an orthogonal wavelet transform on dyadic scales are generally used. For the study of fractals like in this present study, continuous wavelet transforms have been found to be efficient [5]. The wavelet mother has also to be chosen according to the application. When the time series do not have any characteristic scales, or when the goal is to identify discontinuities or singularities, a real wavelet mother has to be chosen. In this

work, we use the N successive derivatives of a Gaussian function:

(35)
$$\psi(x) = \frac{d^N}{dx^N} e^{-x^2/2}$$

These functions are well localized in both space and frequency, and have N vanishing moments, as required for a multifractal analysis. The computations have been performed with N=1,2,4,6,8,10 but only the results for N=2 are discussed in detail in this paper. The results for other values of N are very similar denoting the absence of any polynomial component. Furthermore, the case N=2 is generally used for fractal analysis and corresponds to the so-called Mexican Hat function.

3.1. Data setup. We have applied the wavelet-based multifractal approach to the analysis of two sets of atmospheric data. The first set consists in the monthly averages of the NCEP Daily Global Analyzes data [29]. They correspond to times series of geopotential height from January 1948 to June 2005. A spatial average from 60°N to 90°N is performed at 17 levels, from 10 hPa down to 1000 hPa. Then the annual cycle is removed by subtracting for each month the corresponding mean in order to focus our study onto the anomalies. In such way, we will be able to detect and to describe the singularities present in the signal. Typical stratospheric and tropospheric representations are shown at 100 hPa and 700 hPa in Figures 6 and 7.

The second set of data consists in the Northern Annular Modes (NAM) at 17

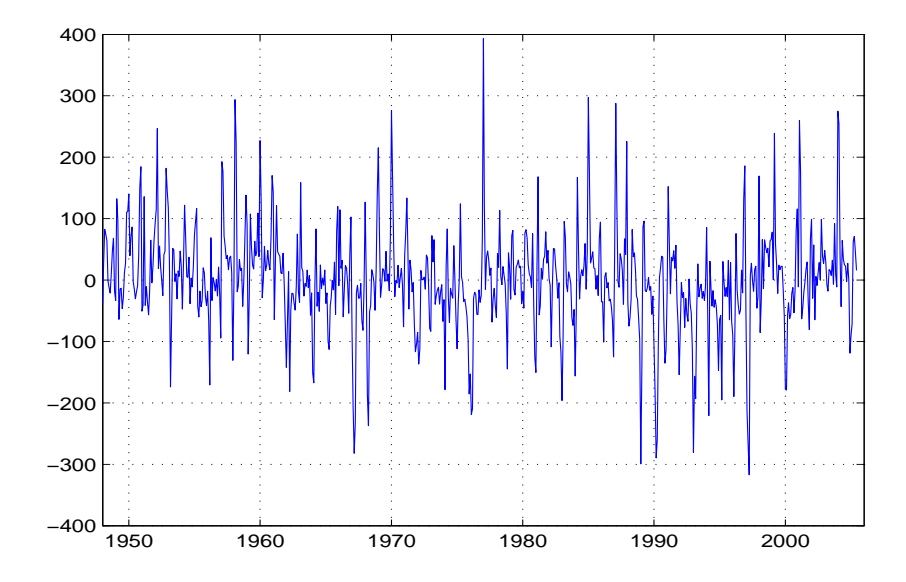


FIGURE 6. 100 hPa monthly anomalies (NCEP) from 60°N to 90°N

levels from the stratosphere down to the surface level from January 1958 to July 2006 provided by Baldwin [6]. At each pressure altitude, the annular mode is the first Empirical Orthogonal Function (EOF) of 90-day low-pass filtered geopotential anomalies north of 20°N. Daily values of the annular mode are calculated for each pressure altitude by projecting daily geopotential anomalies onto the leading EOF

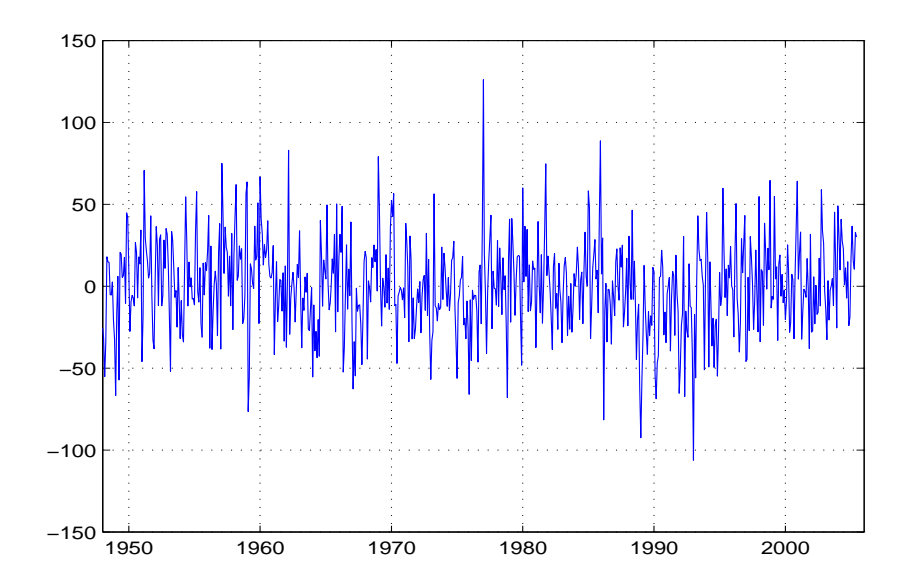


FIGURE 7. 700 hPa monthly anomalies (NCEP) from 60°N to 90°N

patterns. In the stratosphere annular mode values are a measure of the strength of the polar vortex, while the near-surface annular mode is called the Arctic Oscillation (AO), which is recognized as the North Atlantic Oscillation (NAO) over the Atlantic sector.

The results obtained with the second set of data are not given in this paper, and the reader interested in atmospheric sciences can find them in [17].

3.2. Numerical results. The wavelet decompositions obtained with the Mexican Hat function (second derivative of the Gaussian function) are given in Figures 8 and 9. The wavelet transform consists in the calculation of a resemblance index between the signal and the wavelet mother (here the Mexican Hat function). If the signal is similar to itself at different scales, then the wavelet coefficients representation will be also similar at different scales. It can be easily noticed in Figures 8 and 9 that the self-similarity generates a characteristic pattern. This representation is a good demonstration of how well the wavelet transform can reveal the fractal pattern of the atmospheric data. Based only on these representations, we cannot make any significant difference between the stratospheric and the tropospheric signals. But we will see in the sequel by studying the maxima lines of the wavelet transform that these two signals have a different singularity spectrum D(h).

Based on the technical reasons presented in the previous section, the partition function is computed with the formulation given in (16) for q between -20 and 20 with a step size of 0.5.

The first step in the computation of the partition function consists in the detection of the maxima lines of the wavelet transform modulus. The representation of these maxima lines, often called the "skeleton" of the wavelet transform, is given in Figure 10 for the stratospheric signal. For the computation of the partition functions,

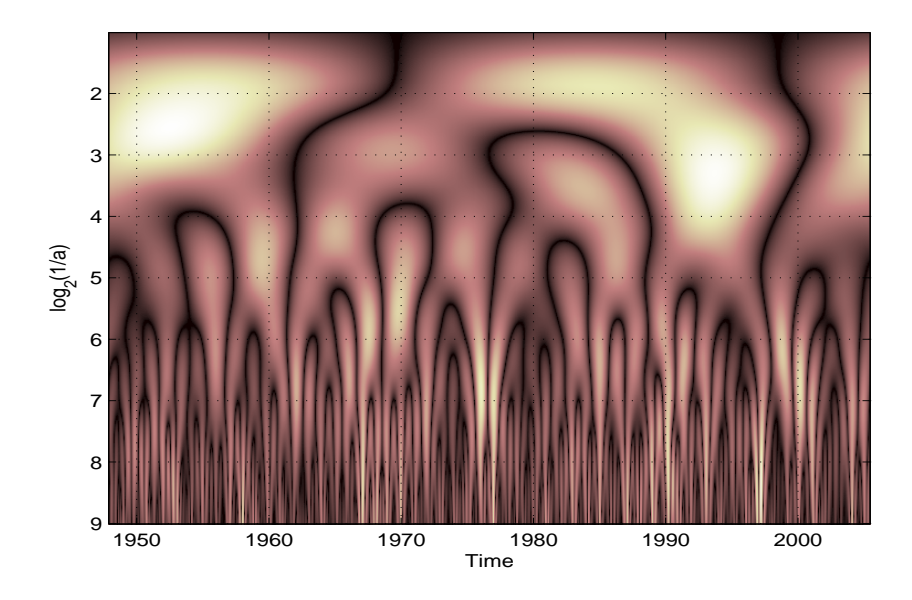


FIGURE 8. Wavelet transform modulus of the 100 hPa signal

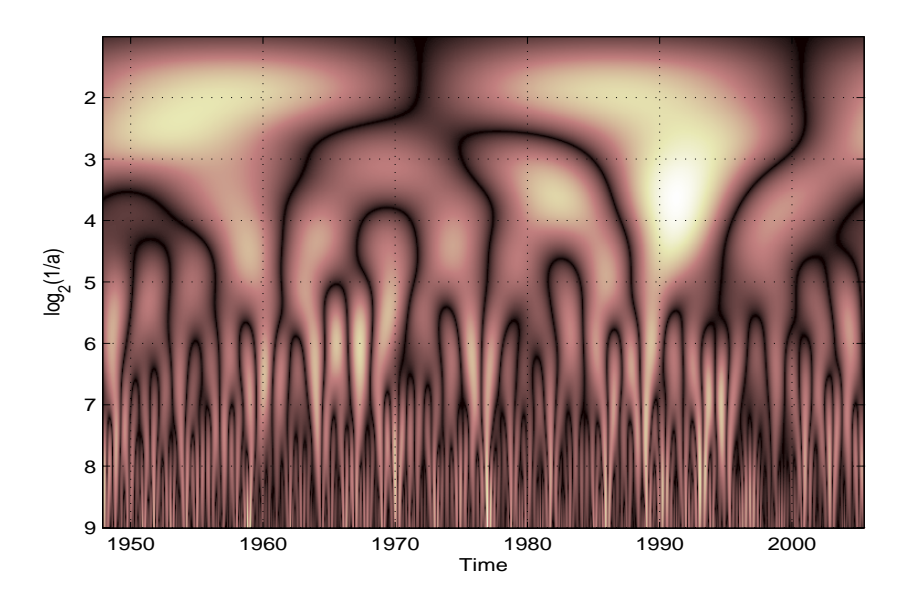


FIGURE 9. Wavelet transform modulus of the 700 hPa signal

only the maxima lines of length longer than 1 octave are kept in the summation in order to keep only the significant singularities. The two partition functions are given in Figures 11 and 12. The steps that can be observed for negative values of q are due to the use of the supremum (otherwise, the computation of Z(q,a) would diverge for negative q). We can remark that the slopes for negative q are different for the stratosphere and for the troposphere. Based on this simple remark, we can

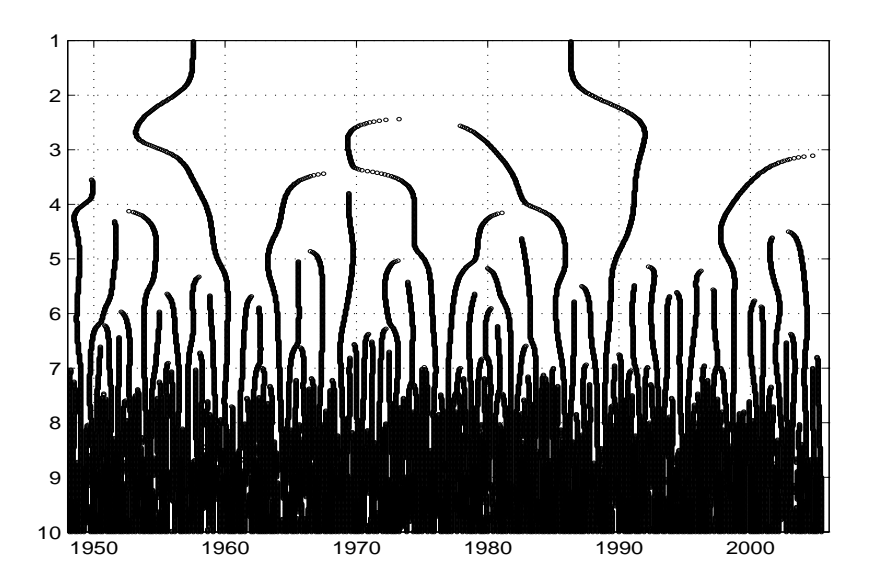


FIGURE 10. Maxima lines of the modulus of the wavelet transform of the $100~\mathrm{hPa}$ signal

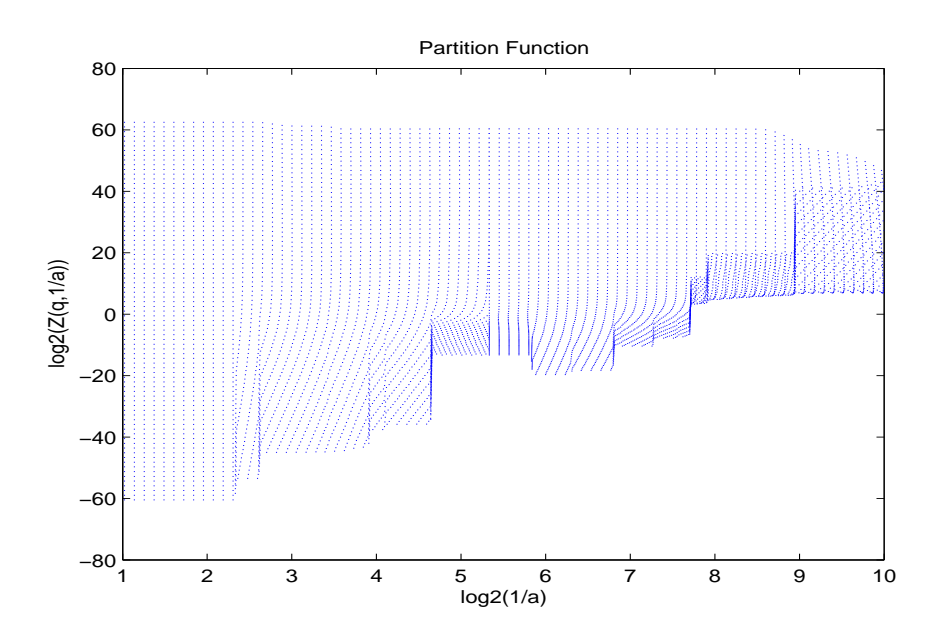


FIGURE 11. Partition function at 100 hPa

already predict that the shapes of the corresponding singularity spectra will be also different. We can expect a steeper down slope in the case of the troposphere. The corresponding singularity spectra are given in Figure 13. The large supports of the spectra prove that the signals are multifractal. A quasi-monofractal signal spectrum would lie on very few values, and a real monofractal signal spectrum

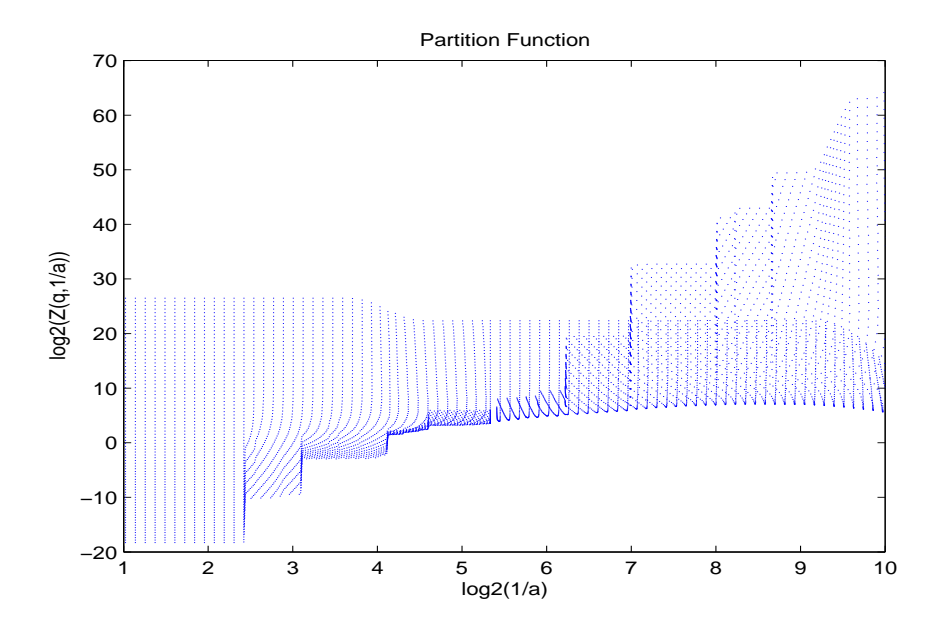


FIGURE 12. Partition function at 700 hPa

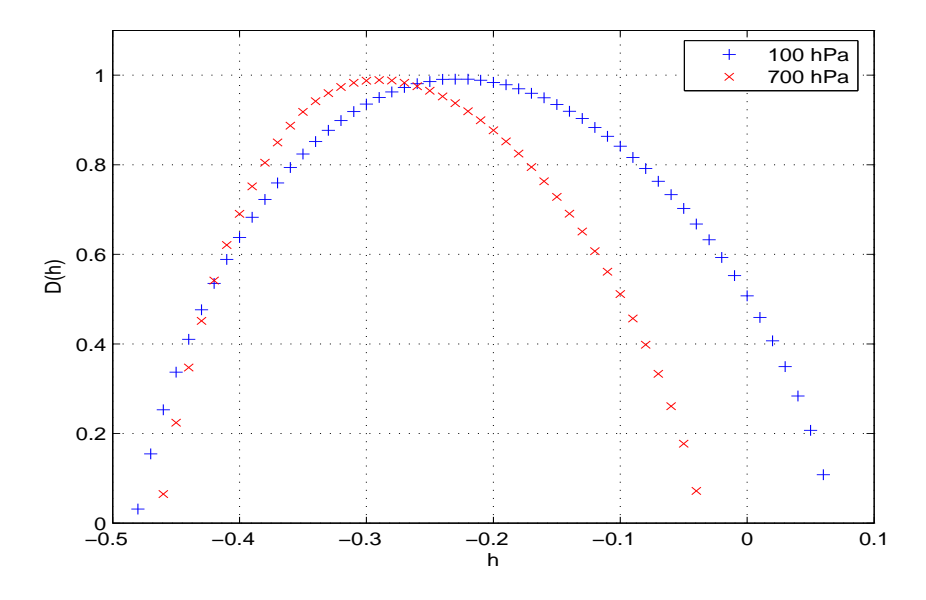


FIGURE 13. Singularity Spectra of the 100 hPa and 700 hPa signals

would reduce to only one point.

As expected, the down slope corresponding to the negative values of q is steeper for the troposphere than for the stratosphere. The maximum of the spectra is obtained around h=-0.29 for the stratosphere and between h=-0.22 and h=-0.23 for the troposphere. We remind here that the smaller is this value the more singular

are the singularities in the signal.

So according to this first study, we can conclude that the singularities in the tropospheric signal are more singular than the singularities in the stratospheric signal. We can verify this first conclusion by computing the value of h where the maximum of D(h) is obtained for the 17 levels from 10 hPa down to 1000 hPa. The results are given in Figure 14. We can clearly detect two areas: the first one with h around -0.23 corresponds to the stratosphere and the second one with h around -0.29 corresponds to the troposphere. These results can be compared to

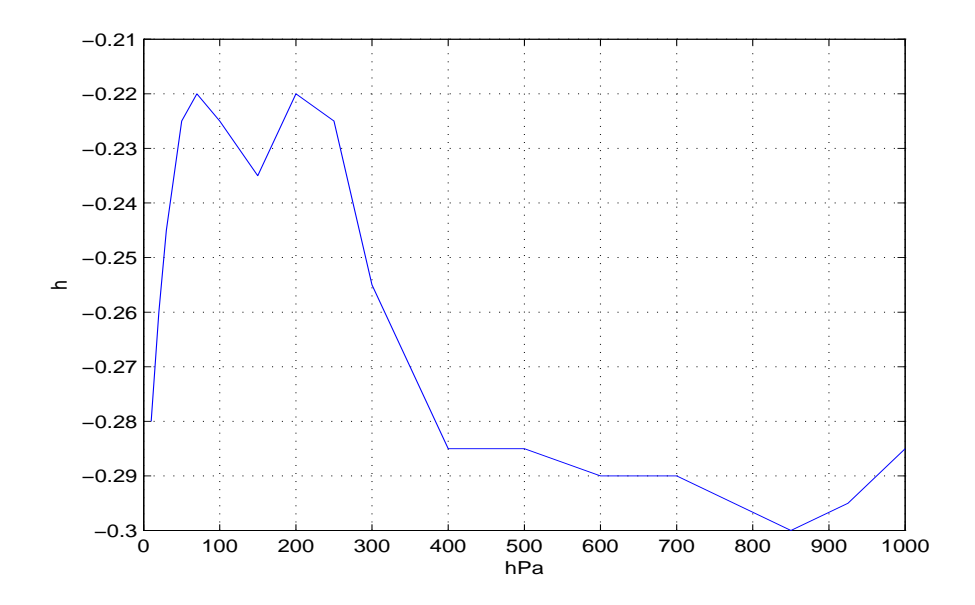


FIGURE 14. Evolution of h in function of the level

the values h obtained for artificial uncorrelated data. We perform the same computations on signals of random numbers whose elements are uniformly disctributed in the interval (0,1). The value of h found for random signals are around -0.4. So with $h \sim -0.3$ or $h \sim -0.2$, the signals corresponding to atmospheric data are close to artificial uncorrelated data at these ranges of time periods.

The whole singularity spectra can also give some information to discriminate stratospheric data from tropospheric data. We can show that their supports are also different as can be noticed from Figure 15. The stratospheric signals present broader spectra than the tropospheric signals indicating the presence of singularities over a larger spectrum.

The analysis performed on the monthly averages NCEP Data cannot give any information for periods smaller than a month. In order to get details on finer time periods, we performed the same kind of analysis on the daily NAM index. the corresponding results are given in [17].

3.3. Discussion. In this part, we have discussed some issues relating to the estimation of the multifractal nature of atmospheric data using a wavelet-based

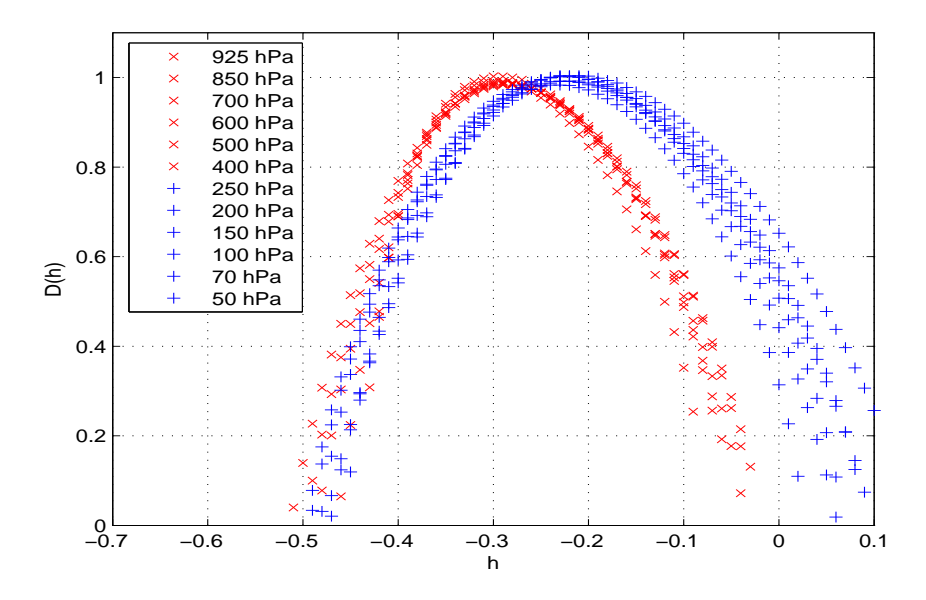


FIGURE 15. Singularity spectra for few levels in the stratosphere and in the troposphere

method. Our study reveals the clear fractal pattern of the analyzed series and their different scaling characteristics. The results obtained with daily data (not shown here) show, in the case of the stratosphere, a short-range correlation behavior that occurs for short range of time scales. In the troposphere and in the same ranges of time, we found a much weaker correlation.

4. Conclusion

Wavelets were developed independently in the fields of mathematics, quantum physics, geology and electrical engineering. They are perfect numerical tools in analyzing physical situations where the signal contains discontinuities or sharp spikes, and they are especially adapted for studying multiscale phenomena in many physical applications. We have shown in this paper a few results obtained in two different problems: two dimensional turbulence, and atmospheric data analysis. In the first application, the wavelet analysis of a two dimensional turbulent flow shows that the vorticity field can be decomposed into two orthogonal subfields. Each subfield is characterized by a distinct structure: vortices or filaments. A more detailed study [14, 15] shows that while the vortical structures are responsible for the transfer of energy upscale, the filamentary structures are responsible for the transfer of enstrophy downscale. In the second application, the continuous wavelet transform allows to enhance the multifractal patterns of the atmospheric geopotential heights. The singularity spectra of the data present different behaviors in the stratosphere and in the troposphere. The connection of the multiscaling properties of atmposheric data to the underlying physical dynamics falls beyond the scope of the present paper. However, by using a two dimensional wavelet transform, we would like to extend our research from time series to spatial patterns of atmosphere analysis.

Acknowledgments

The research was supported by the National Science Foundation, Climate Dynamics Program, under grant ATM-0332364, and the DGA (French Defense Department) under contract 06.60.018.00.470.75.01. P. Fischer would like to thank Dr. D. Casper for many fruitful conversations.

References

- Angot, P., Bruneau, C.H., Fabrie, P. (1999), A penalization method to take into account obstacles in incompressible viscous flows, Num. Math., 81, 497.
- [2] Arneodo, A., Grasseau, G., Holschneider, M. (1988), Wavelet transform of multifractals, Phys. Rev. Lett., 61, 2281.
- [3] Arneodo, A., Bacry, E., Muzy, J.F. (1995), The thermodynamics of fractals revisited with wavelets, Physica A, 213, 232.
- [4] Arneodo, A., Argoul, F., Bacry, E., Elezgaray, J., Muzy, J.F. (1995), Ondelettes, multifractales et turbulence, Diderot Editeur, Paris, France.
- [5] Bacry, E., Muzy, J.F., Arneodo, A. (1993), Singularity spectrum of fractals signal from wavelet analysis: Exact results, J. Stat. Phys., 70, 635-674.
- [6] Baldwin, M.P., http://www.nwra.com/resumes/baldwin/nam.php
- [7] Batchelor, G.K. (1969), Computation of the energy spectrum in homogeneous twodimensional turbulence, Phys. Fluids, 12, 233.
- [8] Bruneau, C.H., Fabrie, P. (1994), Effective downstream boundary conditions for incompressible Navier-Stokes equations, Int. J. Num. Meth. Fluids, 19, 693.
- [9] Bruneau C.H., Kellay H. (2005), Coexistence of two inertial ranges in two-dimensional turbulence. Phys. Rev. E, 71: 046305(5).
- [10] Bruneau, C.H., Mortazavi, I. (2004), Passive control pf the flow around a square cylinder using porous media, Int. J. for Num. Meth. in Fluids 46, 415.
- [11] Bruneau, C.H., Saad, M. (2006), The 2D lid-driven cavity problem revisited, Computers and Fluids, 35, 326.
- [12] Daubechies, I. (1992), Ten lectures on wavelets, CBMS 61, SIAM, Philadelphia.
- [13] Donoho, D. Wavelab802, Software
- [14] Fischer P. (2005), Multiresolution analysis for two-dimensional turbulence. Part 1: Wavelets vs Cosine packets, a comparative study. Discrete and Continuous Dynamical Systems B, 5, 659.
- [15] Fischer P, Bruneau CH, Kellay H. (2007), Multiresolution analysis for 2D turbulence. Part2: A physical interpretation. Discrete and Continuous Dynamical Systems B, 4, 717.
- [16] Fischer P, Bruneau CH. (2007), Spectra and filtering: a clarification, Int. J. Wavelets, Multiresolution and Information Processing, 5, 465.
- [17] Fischer P, Tung KK, Wavelet-based Multifractal Analysis of atmospheric data, Draft version.
- [18] Jaffard, S. (1997) Multifractal formalism for functions Part I: Results valid for all functions, SIAM J. Math. Anal., 28, 944.
- [19] Jaffard, S. (1997) Multifractal formalism for functions Part II: Self-similar functions, SIAM J. Math. Anal., 28, 971.
- [20] Kellay, H., Wu, X.L., Goldburg, W.I. (1995), Experiments with turbulent soap films, Phys. Rev. Lett. 74, 3975.
- [21] Kellay, H., Goldburg, W.I. (2002), Two dimensional turbulence: A review of some recent experiments' Rep. Prog. Phys., 65, 845.
- [22] Kraichnan, R.H. (1967), Inertial ranges transfer in two-dimensional turbulence, Phys. Fluids, 10, 1417.
- [23] Kraichnan, R.H. (1971), Inertial-range transfer in two- and three-dimensional turbulence, J. Fluid Mech., 47, 525.
- [24] Lindborg, E. (1999), Can the atmospheric kinetic energy spectrum be explained by twodimensional turbulence?, J. Fluid Mech. 388, 259.
- [25] Mallat, S., Zhong, S. (1991), Wavelet transform maxima and multiscale edges, in: R.M. B. et al. (Eds.), Wavelets and their Applications, Jones and Bartlett, Boston.
- [26] Mallat, S. (1998) A wavelet tour of signal processing, Academic Press, New York.
- [27] Morel, P., Larcheveque, M. (1974), Relative dispersion of constant-level balloons in 200mb general circulation, J. Atmos. Sci., 31, 2189.

- [28] Muzy, J.F., Bacry, E., Arneodo, A. (1991), Wavelets and multifractal formalism for singular signals: application to turbulence data, Phys. Rev. Lett., 67,3515-3518.
- [29] NOAA-CIRES Climate Diagnostics Center in Boulder, Colorado, USA, http://www.cdc.noaa.gov
- [30] Tung, K.K, Orlando, W. (2003), The k-3 and k-5/3 energy spectrum of atmospheric turbulence: Quasigeostrophic two level model simulation, J. Atmos. Sciences, **60**, 824.
- [31] Wickerhauser, M. V. (1994), Adapted wavelet analysis from theory to software, A.K. Peters, Wellesley, Massachusetts.

Institut de Mathématiques de Bordeaux, Université Bordeaux 1, 33405 Talence Cedex, France

E-mail: Patrick.Fischer@math.u-bordeaux1.fr

 URL : http://www.math.u-bordeaux1.fr/ \sim fischer

Applied Math Dept, University of Washington, Seattle, USA

 $E ext{-}mail: tung@amath.washington.edu}$

 URL : http://www.amath.washington.edu/people/faculty/tung/